The California Baseline Ozone Transport Study (CABOTS)

Ian C. Faloona, Sen Chiao, Arthur J. Eiserloh, Raul J. Alvarez II, Guillaume Kirgis, Andrew O. Langford, Christoph J. Senff, Dani Caputi, Arthur Hu, Laura T. Iraci, Emma L. Yates, Josette E. Marrero, Ju-Mee Ryoo, Stephen Conley, Saffet Tanrikulu, Jin Xu, and Toshihiro Kuwayama

ABSTRACT: Ozone is one of the six "criteria" pollutants identified by the U.S. Clean Air Act Amendment of 1970 as particularly harmful to human health. Concentrations have decreased markedly across the United States over the past 50 years in response to regulatory efforts, but continuing research on its deleterious effects have spurred further reductions in the legal threshold. The South Coast and San Joaquin Valley Air Basins of California remain the only two "extreme" ozone nonattainment areas in the United States. Further reductions of ozone in the West are complicated by significant background concentrations whose relative importance increases as domestic anthropogenic contributions decline and the national standards continue to be lowered. These background concentrations derive largely from uncontrollable sources including stratospheric intrusions, wildfires, and intercontinental transport. Taken together the exogenous sources complicate regulatory strategies and necessitate a much more precise understanding of the timing and magnitude of their contributions to regional air pollution. The California Baseline Ozone Transport Study was a field campaign coordinated across Northern and Central California during spring and summer 2016 aimed at observing daily variations in the ozone columns crossing the North American coastline, as well as the modification of the ozone layering downwind across the mountainous topography of California to better understand the impacts of background ozone on surface air quality in complex terrain.

AFFILIATIONS: Faloona, Caputi, and Hu—University of California, Davis, Davis, California; **Chiao and Eiserloh**—San José State University, San José, California; **Alvarez and Langford**—NOAA/ESRL/Chemical Sciences Division, Boulder, Colorado; **Kirgis and Senff**—CIRES, and NOAA/ESRL/Chemical Sciences Division, Boulder, Colorado; **Iraci, Yates, Marrero,* and Ryoo**—NASA Ames Research Center, Moffett Field, California; **Conley**—Scientific Aviation, Inc., Boulder, Colorado; **Tanrikulu**—Bay Area Air Quality Management District, San Francisco, California; **Xu and Kuwayama**—California Air Resources Board, Sacramento, California
*CURRENT AFFILIATION: Sonoma Technology, Petaluma, California

Air pollution is responsible for over 6 million premature deaths annually worldwide—twice as many as AIDS, malaria, and tuberculosis combined (Landrigan et al. 2018). It is estimated that air pollution directly contributes to more than 200,000 premature deaths per year in the United States (Caiazzo et al. 2013). Many of these deaths are linked to fine particulate matter (PM), but ozone (O_3) plays a central role in most air quality issues because it is the principal source of hydroxyl (OH) and nitrate (NO_3) radicals, the leading agents of atmospheric oxidation, which produce PM and other components of photochemical smog. Moreover, tropospheric ozone is an important greenhouse gas with a radiative forcing of 0.4 ($\pm$0.12) W m^{-2}, just shy of methane (CH_4) (Myhre et al. 2013) and is a phytotoxic pollutant that impacts agricultural yields and tree growth (Lapina et al. 2016). Long-term exposure to O_3 has been implicated in the development of asthma in children (McConnell et al. 2002) and reduced cognitive performance in the elderly (Zhang et al. 2018).

Tropospheric ozone originates from both natural and anthropogenic sources and is photochemically produced by the autocatalytic oxidation of carbon monoxide (CO) and volatile organic compounds (VOCs) in the presence of nitrogen oxides ($NO_x \equiv NO + NO_2$). Natural sources include direct injection from the stratosphere and secondary production from emissions of nonanthropogenic origins such as biogenic VOCs (BVOC) emitted by vegetation (Sindelarova et al. 2014) and NO_x from unmanaged soils (Vinken et al. 2014) and lightning (Zhang et al. 2003). Wildfires (see sidebar "Do wildfires influence O_3, where and by how much?") are another growing source of both NO_x and VOCs (Andreae and Merlet 2001; Jaffe and Wigder 2012). Because the principal loss of ozone requires photolysis followed by reaction with water vapor, and water vapor mixing ratios decrease dramatically with height due to the Clausius–Clapeyron relation, the photochemical lifetime of ozone is altitude dependent and ranges from 1 week in the marine boundary layer (Conley et al. 2011) to 1 year in the upper troposphere (Kley et al. 1996). With a global average lifetime of about 3 weeks (Young et al. 2013), the ozone observed directly upwind of the U.S. West Coast can therefore include anthropogenic contributions transported from East Asia and Europe, and even ozone that originated in the United States but has circumnavigated the globe. This so-called "baseline" ozone constitutes a significant fraction of the ambient concentrations measured in the western United States. Here we conform to the definition proposed by the Task Force on Hemispheric Transport of Air Pollution (HTAP) and adopted in the recent review by Jaffe et al. (2018): "Baseline ozone is defined as the observed ozone at a site when it is not influenced by recent, locally emitted or anthropogenically produced pollution (HTAP 2010)." "Background" ozone, on the other hand (including, for example, North American Background, or Policy Relevant Background), is a model estimate of the O_3 abundances calculated when the anthropogenic precursor emissions from specific areas are omitted or "zeroed out." Throughout this work we will use the term "baseline" due to the observational emphasis of the study.

Do wildfires influence O$_3$, where and by how much?

Fires generate smoke (fine particulates or PM2.5) and a variety of gaseous compounds, including NO$_x$ and VOCs, the photochemical precursors of O$_3$. The net production of O$_3$ by wildfires is highly variable, however, with many contradictory observations reported in the literature (Jaffe and Wigder 2012). The NO$_x$ and VOC emission rates depend on many factors including fuel type and combustion temperature, and the subsequent production of O$_3$ depends on the plume injection height, smoke density, and cloud cover. The amount of O$_3$ within a given smoke plume also varies with distance from the fire. Measurements made near active fires sometimes show a decrease in O$_3$ relative to baseline concentrations because of titration by NO (and possibly reduced NO$_2$ photolysis rates in the shade of the smoke plume), and measurements made far downwind often show little additional O$_3$ production if the NO$_x$ has been depleted or sequestered into more stable compounds like peroxyacetyl nitrate (PAN). The >132,000-acre (>534-km^2) Soberanes fire was the largest wildland fire in California during 2016. The National Interagency Fire Center estimated it to be at the time the most expensive wildland fire in U.S. history with suppression costs exceeding $262 million. The fire was started on the morning of 22 July by an illegal campfire in Garrapata State Park on the windward side of the Coast Range along California's Big Sur coast. It spread southeast from there over the next 10 weeks and by mid-August was burning along the perimeter of the Oliver Observing Station at Chews Ridge (Fig. SB1). The fire burned more than 57,500 acres (232 km^2; 40% of the final burn area) during the first 2 weeks, and smoke from the fire filled much of the central SJV by the last week of July when the highest surface ozone values of 2016 were recorded.

Fig. SB1. Three views of the Soberanes fire taken during CABOTS. (top left) View from Scientific Aviation, Inc., Mooney aircraft looking northward from Chews Ridge. (bottom left) View toward the southwest from the Oliver Observing Station on Chews Ridge (photo credit: Chris Reed, observatory caretaker). (right) MODIS satellite image of the fire from 26 July 2016 (https://earthobservatory.nasa.gov/images/88483/wildfire-along-the-california-coast).

The western United States is particularly susceptible to transported ozone because of several physical factors. First, the baroclinicity induced by the North American coastline at the end of the North Pacific storm track, coupled with the planetary wave activity of the adjacent cordillera, promotes cross-tropopause transport of stratospheric ozone in this region (Sprenger and Wernli 2003). This process peaks in the spring but can occur throughout the year (Škerlak et al. 2014). Second, synoptic-scale subsidence in the lee of the Pacific subtropical anticyclone draws both naturally occurring ozone and transported pollution [including ozone and its precursors such as peroxyacetylnitrate (PAN)] from the middle and upper troposphere toward the surface (Hudman et al. 2004). And third, the deep convective atmospheric boundary layers (ABLs) of the interior West provide stronger coupling between the free troposphere (FT) and the surface (Langford et al. 2017). This direct convective entrainment is strongest during the summer months above arid and/or high-elevation surfaces but is weaker within California's Central Valley where the unusually shallow ABLs are deepest in the springtime (Bianco et al.

2011) and decrease markedly during summer as a result of mesoscale subsidence induced by the mountain–valley circulation (Trousdell et al. 2016) and irrigation practices (Li et al. 2016).

Several modeling studies (Brown-Steiner and Hess 2011; Liang et al. 2004) have shown that the trans-Pacific transport of anthropogenic ozone from Asia is fundamentally different in spring and summer. Episodic long-range transport from Asia increases in frequency with altitude, and peaks in the late spring (April–June) when the prevailing westerlies are strong and extratropical cyclone activity is highest (Lin et al. 2012a). During the summer, much of the Asian pollution is lofted into the upper troposphere (>5 km) by deep convection associated with the East Asian summer monsoon. This summertime ozone is then transported eastward by the prevailing westerly winds aloft, often remaining well above the Coast Range and the Sierra Nevada; however, some is brought downward in the quasi-isentropic flow equatorward and toward the elevated diabatic heating of the mountains.

Despite an estimated reduction in anthropogenic ozone enhancements above baseline levels by a factor of 5 since 1980 (Parrish et al. 2017), California and other western states must continue to achieve significant new emission controls on ozone precursors in order to attain compliance with the current National Ambient Air Quality Standard (NAAQS; see sidebar "Regulatory history of O_3 NAAQS and California standards"). In light of observations indicating rising emissions of ozone precursors from Asia (Sun et al. 2018; Verstraeten et al. 2015), more frequent wild fires (Westerling et al. 2006), and a possible increase in stratosphere–troposphere exchange (Stevenson et al. 2006), concern is mounting about the ability of California and other western states to meet the NAAQS because of a rising baseline component beyond their regional or national regulatory purview.

Numerous modeling (Jacob et al. 1999; Lin et al. 2012b; Pfister et al. 2011) and measurement (Cooper et al. 2011; Jaffe et al. 1999; Parrish et al. 2014; Yates et al. 2017) studies have examined the impact of baseline ozone on surface concentrations across California, but there remains a great deal of uncertainty about the contributions of stratospheric and other transported ozone to surface concentrations in the San Joaquin Valley (SJV), the southern part of the California Central Valley and one of only two "extreme" ozone nonattainment areas remaining in the United States (U.S. EPA Green Book, www.epa.gov/green-book). Much of this uncertainty is thought to result from a lack of detailed information about the vertical distribution of ozone. Intermittent measurements by ozonesondes or aircraft do not provide the temporal coverage needed to easily evaluate how well models can determine the fraction of baseline ozone contributing to surface concentrations measured in the SJV, and this deficiency is by no means limited to California. The main objective of the California Baseline Ozone Transport Study (CABOTS) was to observe the daily changes in ozone layering at the coast (approximately upwind of California) and simultaneously the layering in the Central Valley (downwind of the major emission sources and coastal mountains) in order to produce an unprecedented dataset that might serve to promote ensuing modeling studies. Some issues that the novel dataset may help to illuminate include (i) the fidelity with which air quality models represent ozone transport on synoptic, regional, and local scales in complex terrain; (ii) the relative contributions of stratosphere–troposphere exchange, Asian emissions, and wildfires to the abundances and variability observed in the ozone profiles in and around California; and (iii) the extent to which exogenous ozone that has been transported from afar mixes down to surface sites affecting ozone NAAQS violations in the SJV. Because the project was sponsored primarily by the California Air Resources Board (CARB), a state agency, its initial scope is more limited than many federal scale projects in that it did not include observations of a large suite of photochemical reactants nor did it sponsor extensive modeling efforts. This work summarizes the measurements and unique meteorology of California that serve as the context for this novel dataset and attempts to draw attention to its potential utility for future modeling studies of the impacts of long-range transport on global air quality issues.

Regulatory history of O₃ NAAQS and California standards

Exposure to ozone (O_3) can trigger a variety of health problems, including decreased lung function and pulmonary inflammation, especially for children, elderly, and those with preexisting health conditions such as asthma (EPA 2013). To protect human health, the first ambient air quality standards (AAQS) in California were set by the Department of Public Health (DPH) in 1959, which set a 1-h 0.15 parts per million (ppm) limit for photochemical oxidant levels in outdoor air. In 1967, the California Air Resources Board (CARB) was established and was granted authority to set future AAQS for the state. The federal Clean Air Act (CAA) of 1970 established the National Ambient Air Quality Standards (NAAQS), which set thresholds for criteria air pollutant levels in outdoor air (EPA 1970). Ground-level O_3 is categorized as one of the six criteria air pollutants regulated under NAAQS. Since then, California has continued to invest and lead a multitude of air quality and health research projects, including the evaluation of the peer-reviewed scientific literature on health effects of exposure. These activities led to the adoption of new O_3 standards, including the 1-h 0.09-ppm O_3 standard in 1988 when O_3 was identified as the primary link to respiratory health problems within the group of oxidants present in the atmosphere. This was also the year when the state legislature adopted the California

CAA with strategies that include transportation emission control measures. Following the evaluation mandated by the Children's Environmental Health Protection Act of 1999, CARB and Office of Environmental Health Hazard Assessment (OEHHA) recommended a new 0.070-ppm O_3 standard for the maximum daily 8-h ozone average (MDA8) in 2005 based on human health and environmental impact assessments on O_3. In October 2015, U.S. EPA followed suit and adopted the 0.070-ppm threshold for the 8-h O_3 NAAQS. Compliance with the NAAQS is determined by the "ozone design value" or ODV, the 3-yr running average of the fourth highest MDA8 ozone concentration observed each year at a given site. The ODV is a metric of the high end of the ozone distribution and roughly equivalent to the upper 98th percentile. Nonattainment areas must develop a State Implementation Plan (SIP) that demonstrates how new controls will reduce ground-level ozone to levels below the latest health-based standard. As a result of such continued efforts to minimize the adverse effects of O_3, the maximum 8-h O_3 concentration in the South Coast Air Basin (one of the most polluted regions in California), is now a factor of 3 lower (Fig. SB2) despite a threefold increase in the number of passenger cars on the road, doubling of population, and economic growth of over 2 times.
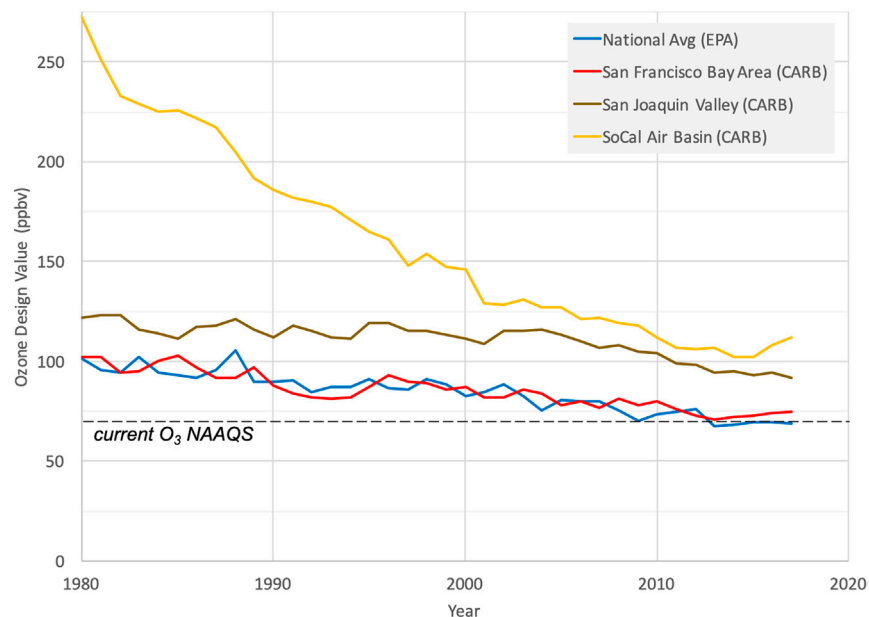

F ɪɢ. SB2. Decadal trends in ozone design values from three different air basins in California compared to the national average and the current NAAQS.

The CABOTS field campaign

Geography. The San Joaquin Valley encompasses the southern two-thirds (~65,000 km²) of the 700-km-long Central Valley of California (Fig. 1). Although it is one of the largest valleys in the world, the geometry and meteorology are not too dissimilar from other places such as the Po Valley in Italy, the San Luis Valley in southern Colorado, the Latrobe Valley in Australia, and the Central Valley of Chile. The 50–100-km-wide San Joaquin Valley is bounded by the Southern Coast Ranges with elevations of less than 1.5 km above mean sea level (MSL) to the
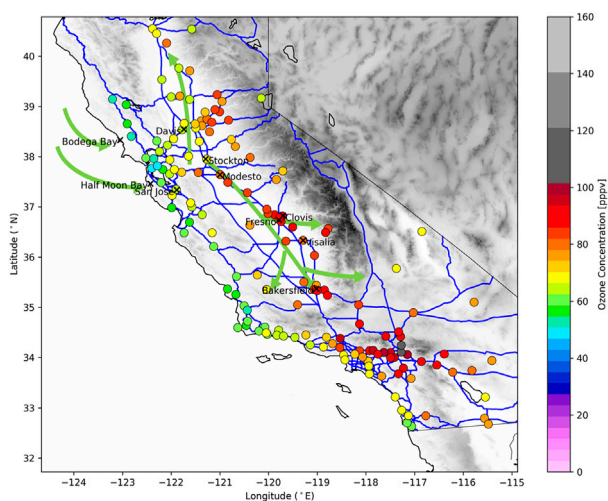
Fig. 1. The 2016 ozone design values (ODV) across the state of California from the CARB surface air quality network. The ODV is defined as the 3-yr running mean of each year's fourth-highest maximum daily 8-h-average (MDA8) ozone concentration. Thin blue lines represent major highways, and thick green arrows show the typical daytime airflow near the surface during the warm season.
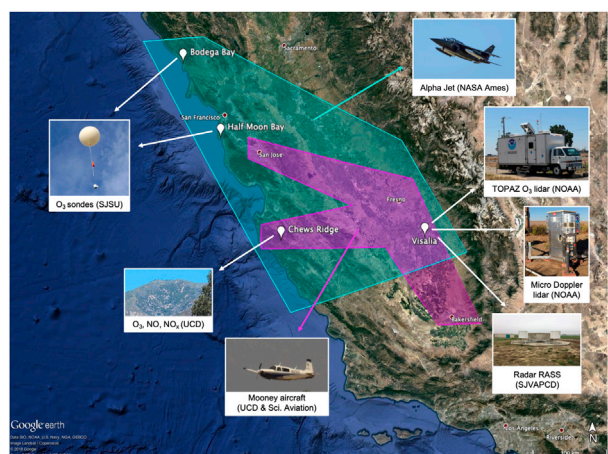
Fig. 2. Overview of CABOTS study domain and measurement platforms ranging from daily ozonesondes launched at the two coastal sites (Bodega Bay and Half Moon Bay) to the NOAA TOPAZ lidar in Visalia. The green and purple polygons represent the approximate domains surveyed by the NASA Alpha jet and Scientific Aviation, Inc., Mooney aircraft, respectively.

west, the Sierra Nevada (<4 km MSL) to the east, and the San Emigdio and Tehachapi Mountains (<2.5 km MSL) to the south. The flat valley floor rises gradually from sea level in the Sacramento–San Joaquin River Delta near Stockton to ~130 m MSL at Bakersfield to the south (see Fig. 1). The SJV is one of the most important agricultural areas in the United States responsible for 12% of all U.S. agricultural production and home to about 10% of California's residents.

Measurement suite. Measurements of ozone vertical profiles by ozonesondes, a ground-based lidar, and aircraft, together with surface ozone concentrations were made from May to August of 2016 (Table 1, Fig. 2). The core measurements included near-daily ozonesonde profiles collected at two sites along the coast and an ozone lidar dataset collected in Visalia, a city of nearly 140,000 residents located deep within the San Joaquin Valley, approximately 60 km southeast of Fresno. Figure 2 shows the locations of the two primary CABOTS ground sites: the ozonesonde launch site at the University of California, Davis, Bodega Marine Laboratory (UCD BML) in Bodega Bay (BBY) and the lidar site at the Visalia Municipal Airport (VMA) on the eastern side of the SJV. The UCD BML (38.319°N, 123.072°W) is located approximately 80 km north of San Francisco, and ozonesondes were launched daily there 6 days per week from the middle of May to the middle of August 2016 by researchers from San José State University (SJSU). Additionally, a second launch site was operated at the same periodicity for a subset of the project at Half Moon Bay (HMB, 37.504°N, 122.483°W) located 25 km to the south of San Francisco.

The National Oceanic and Atmospheric Administration (NOAA) TOPAZ (Tunable Optical Profiler for Aerosols and Ozone) differential absorption lidar (DIAL) system (Alvarez et al. 2011) was operated daily during two 3-week-long intensive operating periods: IOP1 (27 May–18 June) and IOP2 (18 July–7 August). TOPAZ uses a scanning mirror for measurements at different elevation angles to provide quasi-continuous ozone and aerosol backscatter profiles from 25 m to about 6 km above ground level (≥8 km at night). A radar wind profiler and radio acoustic sounding system (RASS) at the Visalia airport provided measurements of virtual temperature profiles up to 1–1.5 km and winds up to 4 km.

In addition to these core measurements, the UCD and Scientific Aviation, Inc. team conducted aircraft measurements to characterize the evolution of ozone layering in the lower atmosphere (<1,500 m) over the course of the entire diurnal cycle from Fresno to Bakersfield. Flights for this separate study investigating the effects of residual layer (RL) ozone and its mixing on surface exceedances overlapped with some of the CABOTS project. Additionally, supplemental

Table 1. Observational overview table.

Parameters observed	Method	Date interval
Bodega Bay, ozonesonde site, (38.319°N, 123.072°W), San José State University		
O_3	Electrochemical concentration cell (ECC)	6 days per week, 16 May–16 Aug
T, RH	Bead thermistor and capacitance hygrometer	
Wind	GPS tracking	
Half Moon Bay, ozonesonde site, (37.505°N, 122.484°W), San José State University		
O_3	ECC	6 days per week, 24 Jul–17 Aug
T, RH	Bead thermistor and capacitance hygrometer	
Wind	GPS tracking	
Chews Ridge, mountain inflow monitoring site, (36.306°N, 121.567°W), University of California, Davis/ Monterey Institute for Research in Astronomy		
O_3	UV absorption (2B-Tech)	1 May–31 Aug
NO/NO_x	Chemiluminescence/photolysis (TECO with Mo converter)	
T, RH, wind speed/direction	Davis Instruments	
Mooney Aircraft, University of California, Davis/Scientific Aviation, Inc.		
O_3	UV absorption (2B-Tech)	2–4 Jun, 28 Jun, 24–26 Jul, 27–29 Jul, 4–6 Aug, 12–18 Aug
NO/NO_x	Chemiluminescence/photolysis (EcoPhysics/Air Quality Design, Inc.)	
$CH_4/CO_2/H_2O$	Picarro CaRDS	
T, RH	Vaisala Instruments	
Horizontal winds	In-house dual GPS (Hemisphere; Conley et al. 2014)	
AJAX, NASA Ames Research Center		
O_3	UV absorption (2B-Tech model 205)	12 May, 19 May, 3 Jun, 15 Jun, 23 Jun, 6 Jul, 21 Jul, and 28 Jul 2016
$CH_4/CO_2/H_2O$	IR cavity ringdown spectroscopy (Picarro model G2301-m)	
3D wind, P, T	NASA Ames MMM package	
HCHO	Nonresonant laser-induced fluorescence (St. Clair et al. 2017)	12 May, 15 Jun, 23 Jun, 21 Jul, 28 Jul
TOPAZ ozone lidar, NOAA/Earth System Research Laboratory		
O_3, aerosol backscatter profiles	Differential absorption lidar (DIAL)	IOP1: 27 May–18 Jun, IOP2: 18 Jul–7 Aug
O_3	UV absorption (2B-Tech model 205)	27 May–8 Aug
T, P, RH, wind speed and direction	Airmar 150WX weather station	27 May–8 Aug

funding was provided by the U.S. EPA to study the afternoon ABL and photochemical ozone production rates in the valley between Fresno and Visalia, upwind of the TOPAZ lidar, on six additional days: 27–29 July and 4–6 August (Trousdell et al. 2019). Furthermore, the Alpha Jet Atmospheric Experiment (AJAX) of the NASA Ames Research Center (Hamill et al. 2016) performs regular missions to measure ozone and greenhouse gases, such as ozone, carbon dioxide (CO_2), methane (CH_4), and formaldehyde (HCHO) over California and Nevada, and was coordinated to contribute to CABOTS. A comprehensive intercomparison of the TOPAZ lidar with both airborne platforms (Langford et al. 2019) found excellent agreement (within 5 ppbv on average) among the three measurements.

In addition to the usual ozone data collected at nearly 80 CARB (25 in the SJV Air basin) routine surface sites in Central and Northern California that are available for the study (www .arb.ca.gov/aqmis2/aqdselect.php), the San Joaquin Valley Air Pollution Control District (SJVAPCD) had funded ozone measurements made by UCD at the Oliver Observing Station (http://tycho .mira.org/oosweather/), which is operated by the Monterey Institute for Research in Astronomy

(MIRA; www.mira.org/) on Chews Ridge. This solar and wind-powered mountain observatory is at an elevation of 1,550 m MSL in the Los Padres National Forest 40 km southeast of Monterey but located about half that distance downwind from the Big Sur coastline to the southwest from whence the winds blow two-thirds of the time (Asher et al. 2018). Measurements of O_3, NO, and NO_x collected at this site during CABOTS are available although much of it was heavily impacted by the Soberanes fire during the second IOP, which burned along the northwest perimeter of the Oliver Observing Station from late July to early October.

Synoptic setting. The SJV has a Mediterranean climate well suited for agricultural production. The winters are usually cool and moist, but the summers are hot and dry with less than 10% of the annual precipitation falling between May and September (https://cdec.water.ca.gov/snow_rain.html). The principal ABL summer wind patterns are dominated by the thermally driven mesoscale circulations of the coupled sea–land and valley–mountain flow. Onshore winds can usually only penetrate into California's Central Valley at breaks in the Coast Range because the marine ABL tends to be well below the height of the coastal mountains (Dorman et al. 2000), and mostly the winds feed in through the Carquinez Strait east of the San Francisco Bay Area (Fig. 1). This inflow is modulated by the synoptic conditions as well as diurnal up-valley winds and by upslope/downslope flow along the flanks of the Sierra Nevada and Coast Ranges (Bao et al. 2008; Zhong et al. 2004). The northwesterly inflow brings ozone and other pollutants from the San Francisco Bay area and Sacramento (Fast et al. 2012) up the valley toward Bakersfield, but also flushes the valley with clean marine air, particularly at night when up-valley winds can strengthen into an elevated low-level jet (LLJ) (Caputi et al. 2019). Some of this flow exits the valley through the Tehachapi Pass 75 km southeast of Bakersfield, but much is blocked by the mountains and recirculated northward where it interacts with cross-valley drainage flows and the LLJ to form an early morning low-level counterclockwise circulation known as the Fresno eddy (Bao et al. 2008; Lin and Jao 1995), which is believed to foster the buildup of ozone in the SJV (Beaver and Palazoglu 2009).

The daytime upslope winds carry ozone and other pollutants from the SJV into the surrounding mountains (Panek et al. 2013) with the circulation closed by elevated compensation flows above the valley (Zardi and Whiteman 2013). Subsidence created by this mountain–valley circulation and the synoptically persistent North Pacific high (Trousdell et al. 2016), and to a lesser extent, evaporative cooling associated with widespread agricultural irrigation (Li et al. 2016), limits the growth of the convective mixed layers (ML) in the central SJV to ~1 km or less during summer (Bianco et al. 2011) with somewhat deeper mixed layers in the southern part of the valley where the converging up-valley flow is lifted by the weir of the Tehachapi Mountains (Trousdell et al. 2016). The sidewall venting creates elevated pollution layers above the ML that spread across the valley when the synoptic forcing is weak (Fast et al. 2012; Leukauf et al. 2016). Ozone remaining in the residual layer left after the ML decays can be reentrained the following day or turbulently mixed into the stable nocturnal boundary layer by the LLJ and destroyed at the surface (Caputi et al. 2019). Above the average daytime ABL height (500–600 m), there exists an intermediate layer, composed of a mixture of free-tropospheric inflow coming over the coast range and air lofted above the ABL by the sidewall slope flows. Because this region is a mixture of baseline FT air and surface-influenced ABL air, and because it is stably stratified yet intermittently turbulent (Faloona 2018) we refer to it as a buffer layer (BuL) similar to that described by Russell et al. (1998) over the ocean.

The synoptic and mesoscale subsidence associated with the Pacific high and mountain–valley circulation also inhibits cloud formation during the summer, and the combination of high temperatures and clear skies in July and August fosters rapid photochemical production of O_3 from NO_x and VOC precursors transported into the valley by the northwesterly inflow, emitted by urban sources, or released by distributed transportation, agricultural,

and petrochemical sources within the SJV (Trousdell et al. 2019; Pusede et al. 2014). To some degree the Fresno eddy recirculates these pollutants within the southern SJV to help create an ozone hot spot near Fresno (Beaver and Palazoglu 2009), although the strong associated low-level jet may also induce vertical mixing at night that depletes ozone (Caputi et al. 2019).

Synoptic charts of reanalysis data for both TOPAZ IOPs, as well as a June–August average for 2010–15, are shown in Fig. 3 [data from the National Centers for Environmental Prediction's (NCEP) North American Regional Reanalysis (NARR); www.esrl.noaa.gov/psd/cgi-bin/data/narr/plotday.pl]. On the 900-hPa (≈1 km MSL) geopotential height fields, the synoptic patterns for both IOPs are seen to closely resemble the climatological pattern, with a thermal low over the southern California–Nevada border and alongshore, equatorward winds over the ocean. A mean up-valley (northwesterly) flow is present in the SJV due to the mountain–valley circulation, but is geostrophically reinforced by the pressure gradient between the offshore Pacific high and inland thermal low.
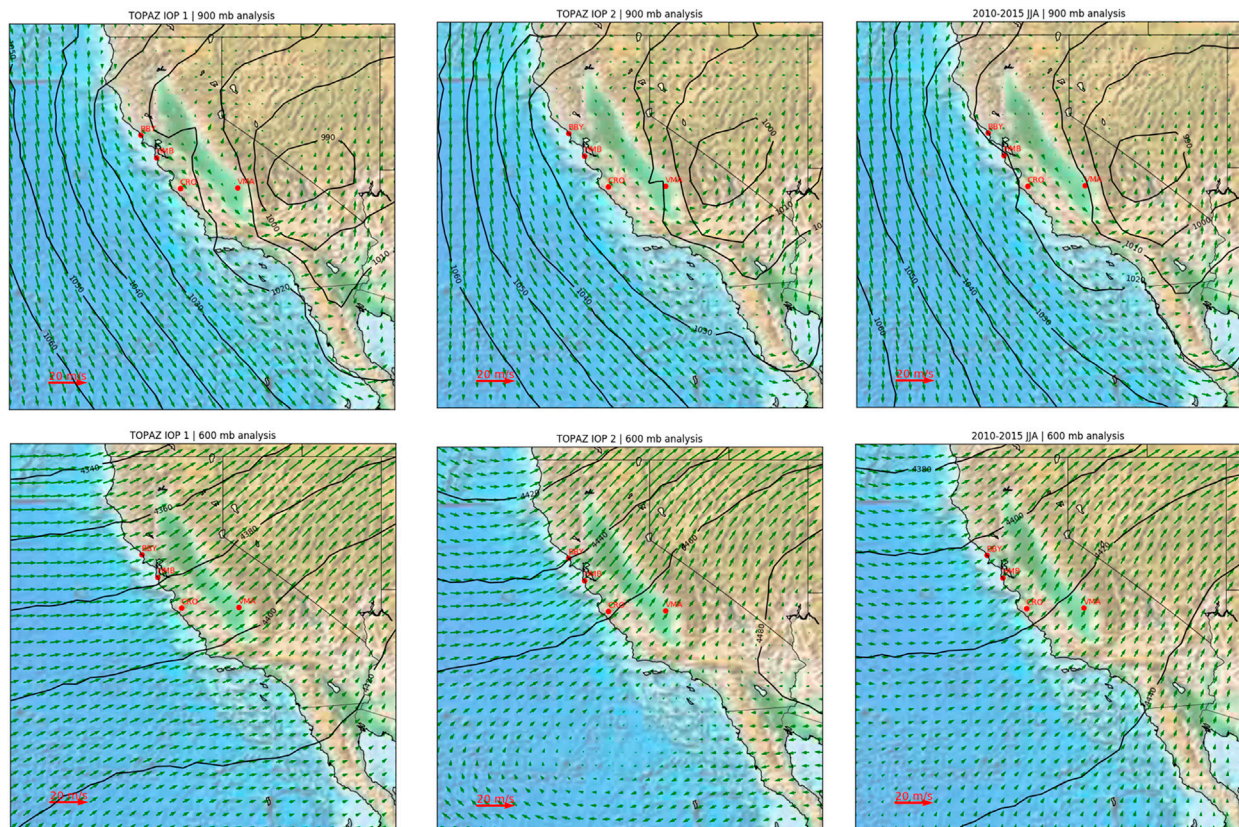
Fig. 3. Geopotential heights for CABOTS at (top) 900 and (bottom) 600 hPa for (left) IOP1, (center) IOP2, and (right) climatological average for June–August 2010–15. The two pressures are near the altitudes of maximum correlation found between O$_3$ observations at Bodega Bay (BBY) and Visalia Municipal Airport (VMA).

Figure 4 shows the monthly average tropospheric column ozone concentrations derived from the difference between the total column ozone measured by the NASA *Aura* Ozone Monitoring Instrument (OMI) and the stratospheric column measurements made by the *Aura* Microwave Limb Sounder (MLS) (Ziemke et al. 2006) during the three core months of the CABOTS project. Superimposed on the tropospheric-averaged concentrations are the NCEP reanalysis winds at the 300-hPa isobaric level for each month considering that the main summertime trans-Pacific transport is centered aloft near 8 km (Brown-Steiner and Hess 2011). The patches of elevated ozone over the central Pacific in June and the faster winds may represent the trailing
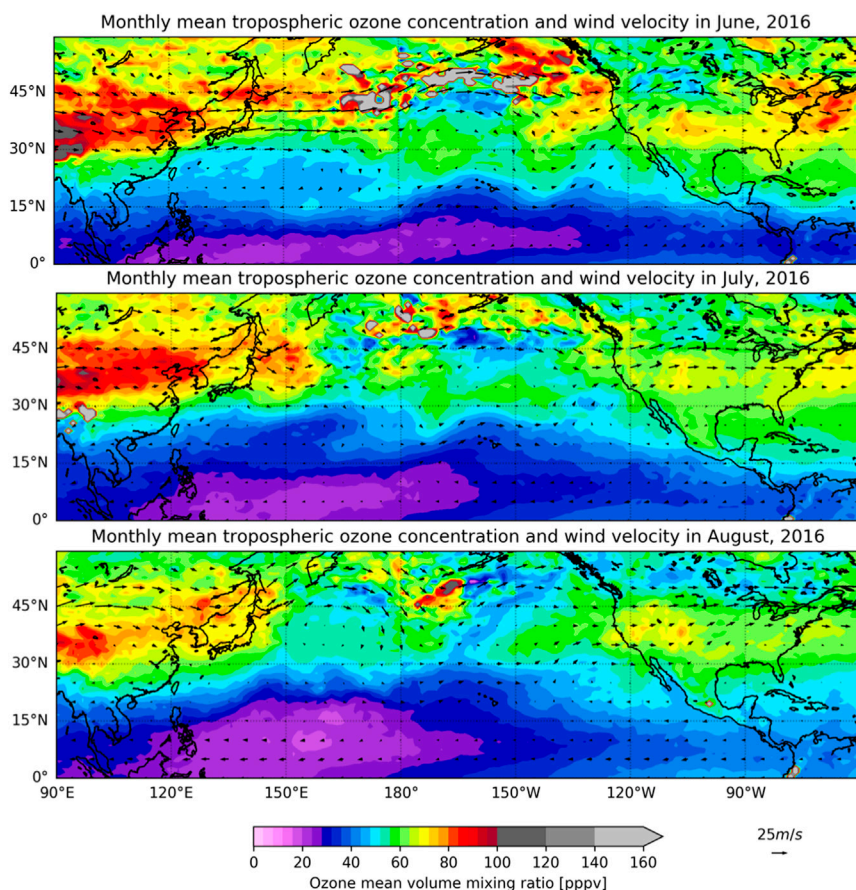
Fig. 4. NASA Goddard tropospheric column O$_3$ product from *Aura* OMI/MLS and the NCEP Reanalysis winds at 300 hPa for each of the summer months of the CABOTS project.

edge of springtime baroclinicity in the midlatitudes, which is often accompanied by enhanced stratosphere–troposphere exchange. The seasonal progression of Fig. 4 also shows the poleward advancement of the ITCZ with its depleted ozone and easterly winds that shunt the main Asian effluent northward throughout the summer season. Interannual variations in this advancement associated with the Pacific decadal oscillation (PDO) have been shown to markedly influence the long-term trends in ozone observed at the baseline site on Mauna Loa, Hawaii (Lin et al. 2014).

Some examples of the CABOTS measurements

The curtain plot of Fig. 5 shows the daily ozonesonde data from both the Bodega and Half Moon Bay sites. The daily data exhibit patterns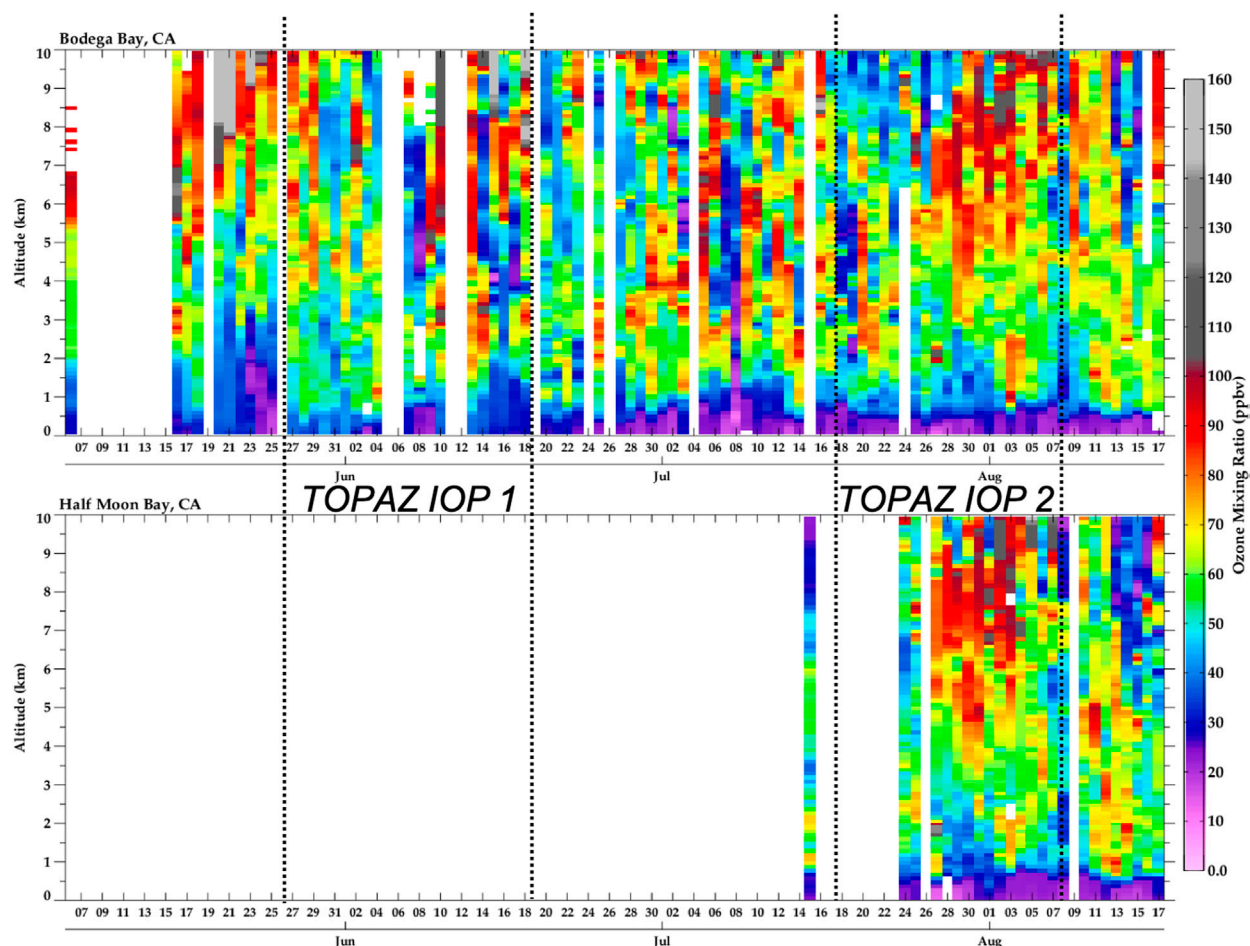 similar to those seen in the Trinidad Head (THD) analyses of less frequent (weekly) soundings over a decade reported by Oltmans et al. (2008), with undulations of ozone concentrations in the mid- to upper troposphere of 3–5-week periodicities. A comparable ozonesonde study by Cooper et al. (2011) coordinated with the CalNex campaign (Ryerson et al. 2013) reported the ozone percentile distributions observed in near-daily profiles above THD (320 km north along the coast from Bodega Bay) for 5 weeks (10 May–19 June) during 2010. At 2 km the 5th, 33rd, 50th, 67th, and 95th percentiles were found to be 30, 44, 47, 51, and 62 ppbv (their Fig. 10). Figure 5 shows three or four episodes of enhanced ozone in the upper troposphere at BBY and the depletion of marine ABL ozone, below about 500 m, as the summer progresses due to photochemical destruction in a more or less pristine environment. The observed day-to-day variability does appear to be larger during the 3-month interval of CABOTS, which shows the 5th, 33rd, 50th, 67th, and 95th percentiles at 2 km to be 36, 51, 57, 62, and 77 ppbv. The 10-ppbv greater median ozone at 2 km above BBY than at THD is consistent with the upward-sloping meridional isopleths reported in Cooper et al. (2011). The larger interquartile range may be due to the longer interval of the CABOTS dataset, but is indicative that day-to-day variability is important for accurately constraining the oxidant boundary conditions along the North American inflow. To take a preliminary look at how well a commonly used chemical transport model captures the ozone amounts and variability as a chemical boundary condition, a comparison of the observed mean and standard deviation profiles (black) with those generated in the Model for Ozone and Related Chemical Tracers (MOZART; Emmons et al. 2010) (red) is shown in Fig. 6 for the 24 ozonesondes launched between mid-July and mid-August at the HMB site. While the model does capture the strong gradients at the top of the marine ABL well, there does seem to be a systematic 5–15-ppbv underestimate throughout most of the

Fig. 5. Ozonesonde profiles measured at (top) Bodega Bay and (bottom) Half Moon Bay during CABOTS (vertical dashed lines indicate TOPAZ IOPs).

troposphere followed by overpredictions greater than 20 ppbv above 10 km (not shown). It is also important to note that in the region between 1 and 3 km, which likely influences the surface ozone levels in the interior Central Valley and wes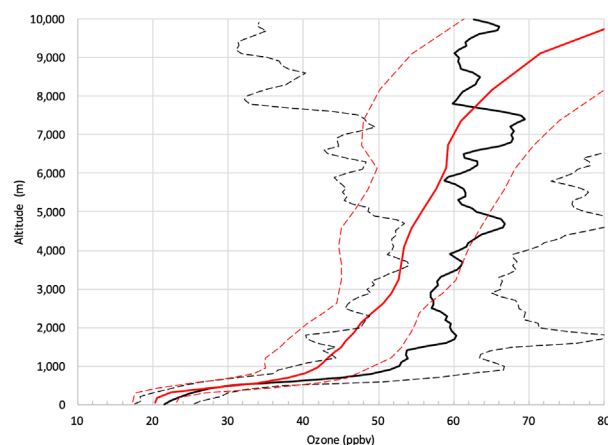tern face of the Sierras the most, the observed day-to-day standard deviation is ~60% greater than is captured in the model. Furthermore, in agreement with the findings presented in Fig. 6 of frequent ozone concentrations well above 60–70 ppb (mean plus one standard deviation) at 1.5-km altitudes and above, an analysis of the ozone time series collected at Chews Ridge from 2012 to 2014 determined that the ODV for this remote site located in a National Forest in the coastal mountains was 70.5 ppbv, technically in violation of the NAAQS.

Figure 7 shows the compiled time series from the TOPAZ ozone lidar at Visalia over the course of the two IOPs. The scalloped appearance of the daily curtain plots is caused by increased solar background radiation near local noon, which reduces the lidar maximum range. In general, the lidar data show the rich textures of the air above the valley with

Fig. 6. Mean (solid lines) and plus and minus one standard deviation (dashed lines) of the observed ozone (black) and the model ozone from MOZART (red) above the Half Moon Bay site. The comparison is for 24 days between mid-July and mid-August 2016.

frequent episodes of high ozone advected overhead in the upper troposphere (also seen in Fig. 5), as well as synoptic accumulations of ozone in the ABL, but also in the buffer layer above up to 2–2.5 km. Generally, the features appear to slope downward over the course of several days as would be expected with isentropic (westerly) flow over the heated (and better mixed) continental atmosphere.

The TOPAZ measurements from IOP2 are also presented as diurnally averaged profiles in Fig. 8. Only the diurnal hours with more than 5 days of measurements are shown. The statistics are most robust for the hours between 1300 and 1900 PDT when more than 12 days of measurements are averaged. The corresponding mean winds from the collocated SJVAPCD profiler are superimposed on each plot; wind speeds less than 2 m s^{-1} are represented by crosses. The wind vectors show the horizontal wind direction with the top of the plot representing north and the right side representing east (arrows that point to the right in the figure therefore represent *westerly*
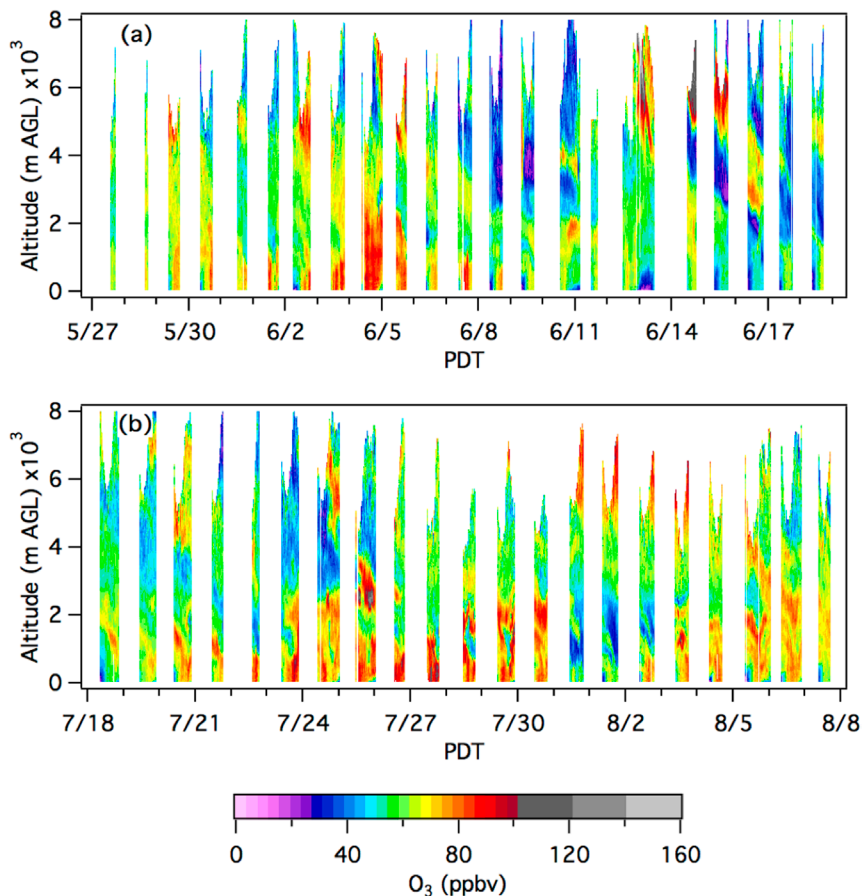

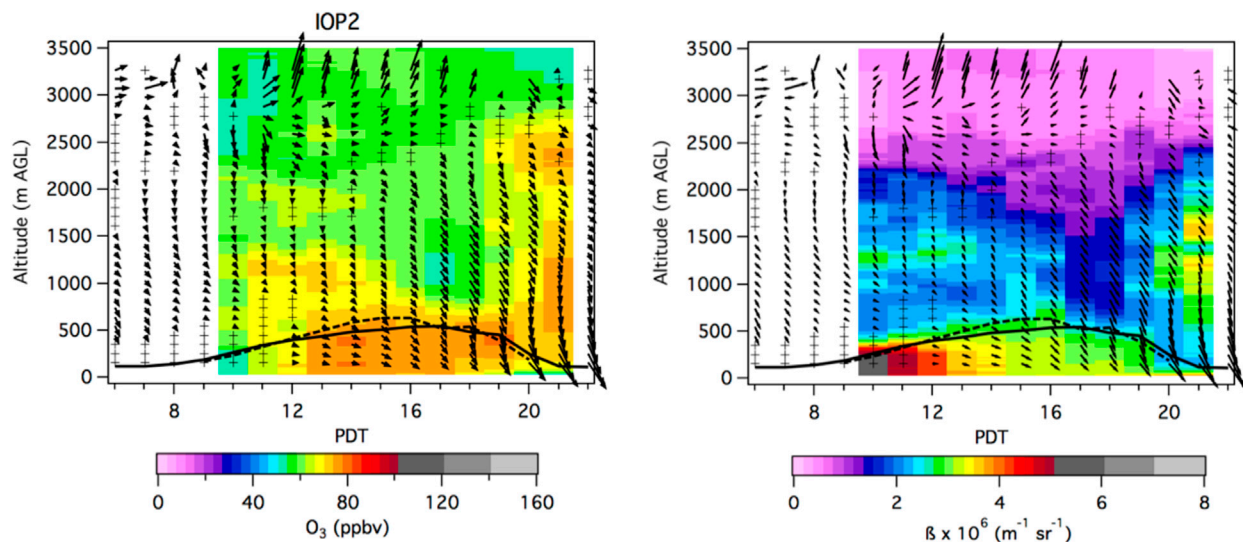Fig. 7. TOPAZ O$_3$ lidar profiles for (a) IOP1 and (b) IOP2.

Fig. 8. Mean diurnal profiles of TOPAZ (top) ozone and (bottom) backscatter, along with winds from the collocated SJVAPCD radar profiler and RASS during the second CABOTS IOP. The black lines show the ABL height inferred from the RASS temperature profiles (solid) and a collocated NOAA Doppler lidar (dashed).

winds). The mean winds, primarily northwesterly throughout a deep layer (ABL + BuL) during daytime, begin westerly (upslope) in the late morning and grow stronger and more northerly in the afternoon ABL as the up-valley thermal circulation prevails. The general pattern appears very similar to those shown in Zhong et al. (2004) and Bao et al. (2008) that were based on data collected at Visalia during the 2000 Central California Ozone Study. The solid black line in each plot represents the ABL height calculated from gradients in the RASS virtual temperature profiles. The dashed line in Fig. 8 shows the ABL height calculated from direct measurements of the vertical velocity variance by an experimental NOAA/ESRL Doppler lidar deployed next to TOPAZ during the last 2 weeks of the campaign. These two independent measurements are in very good agreement and are also consistent with the gradients observed in the TOPAZ UV backscatter profiles. All three methods indicate that the mean ABL height of ~500 m at Visalia corresponds fairly well to the reported average afternoon ABL heights of 550 m for the region between Visalia and Fresno (Trousdell et al. 2019) during the six EPA flights of the Scientific Aviation Mooney. The diurnally averaged O_3 data for IOP2 show depletion overnight in a shallow nocturnal boundary layer due to nitrate production and dry deposition (Caputi et al. 2019) followed by a well-mixed buildup of O_3 in the ABL during the day. The prevalence of elevated ozone (>70 ppb, orange colors) between 500 and 2,500 m in these average profiles of Fig. 8 is evidence that ABL air is lofted into the buffer layer above due to daytime slope flow along the flanks of the valley during its up-valley progression toward the southeast. Further evidence of this slope venting is presented for other scalars in the discussion surrounding Fig. 10 that follows. Note that this buffer layer lies above any residual layer left behind when the convective mixed layer decays in the evening. The accumulation of afternoon lofting is especially evident in Fig. 8 at 2100 PDT.

Another representation of the three-layered valley atmosphere is illustrated in Fig. 9, which shows a terrain cross section running from the coast near Chews Ridge perpendicular to the valley axis into the Sierra Nevada (topography data from the NASA Shuttle Radar Tomography Mission). Winds from the Half Moon Bay ozonesondes are plotted along the coast, and those averaged from the Visalia RASS from 1200 to 1600 PDT during July–August at the corresponding cross-valley axis distance. Vector averaged winds are represented by the arrows (with north oriented toward the top of the page), and scalar average wind speeds are displayed by the arrow color. The red and the blue lines are average potential temperature and ozone, respectively, measured by the Mooney aircraft during the six EPA flights. These data show an average ABL height of ~600 m wherein the afternoon ozone tends to be the highest, and then distinctly show an intermediate, statically stable BuL where the ozone concentrations are somewhere between ABL and free-tropospheric (above ~2,000 m) amounts. These data show the typical southwesterly flow at Chews Ridge entering the
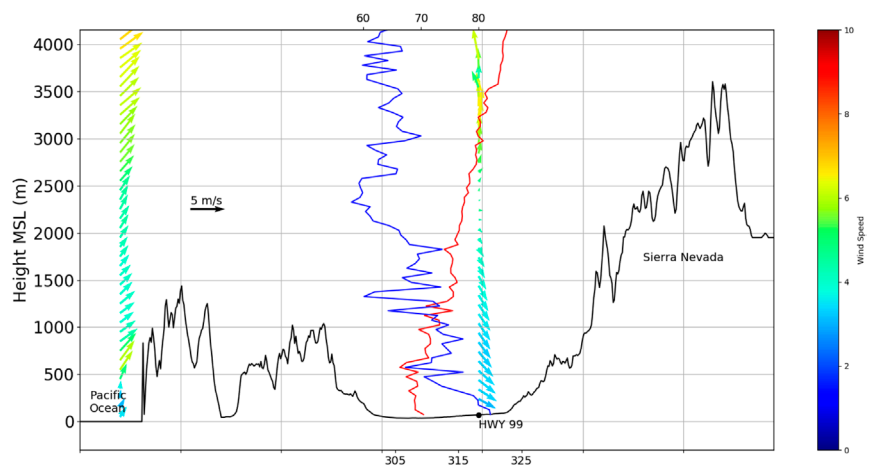
Fig. 9. Cross section of SJV through the Chews Ridge site passing across California Highway 99 between Madera and Merced (approximately 100 km north of Visalia). Vector average winds as a function of height and mean scalar wind speed (colors), shown with respect to north directed straight up, from the coastal wind profile observed by sondes at Half Moon Bay (approximately 100 km north of Chews Ridge) and at Visalia by the RASS for 1200–1600 PST during July–August 2016. Ozone (blue) and potential temperature (red) are averages from the afternoon Mooney aircraft flights profiling throughout the region.

valley over the coastal ridgeline, but as the air travels inland it is swept up into the up-valley (northwesterly) wind of the SJV that dominates from the surface all the way to the top of the buffer layer. Somewhere between 2,000 and 2,500 m the vector wind average is almost the null vector, a near balance of up- and down-valley winds, with an average scalar wind speed near 4–5 m s^{-1}, similar to the onshore flow at the same level. Thus, the presence of the high southern Sierra Nevada downwind appears to block the flow's progression, but does not stagnate as much as recirculate the air within the valley buffer layer. Higher up, in the free troposphere, the obstruction of the mountains also impedes the flow, weakening the Coriolis force, but above the reach of the mountain–valley thermal circulation air is pushed down the background pressure gradient (Fig. 3), which is directed more or less down-valley, driving southeasterly winds aloft. Note that despite the well-defined thermodynamic capping inversion atop the valley boundary layer, there is little wind shear across the inversion as the daytime up-valley flow persists throughout the ABL and BuL.

A more instantaneous picture of the valley atmosphere's layering can be seen in Fig. 10 showing NASA AJAX spiral/vertical profile at the coastal BBY site (dark purple) compared to the inland profile flown near Visalia (cyan) only 30 min later on 15 June. Because the AJAX flight was scheduled for the morning, the ozonesonde was launched at BBY early to be nearly coincident at 1000 PDT. The five scalars shown (from left to right: CO_2, CH_4, O_3, H_2O, and HCHO) clearly indicate the difference between the baseline composition of the air moving onshore at the coast and the air heavily influenced by California's Central Valley. In this instance, the ABL at Visalia appears to be 200–300 m, a RL up to about 800 m, and the buffer layer seems to extend up to about 2,500 m. The long chemical lifetime and strong surface sources of CH_4 from agriculture and oil production in the SJV (Trousdell et al. 2016) clearly show the layering of an ABL/RL with methane enhanced by 100–150 ppbv over the baseline observed offshore. The secondary enhancements of CH_4 at 1,500 and 2,300 m clearly show the lofting of ABL valley air into the buffer layer that had occurred most likely on the previous afternoon when western
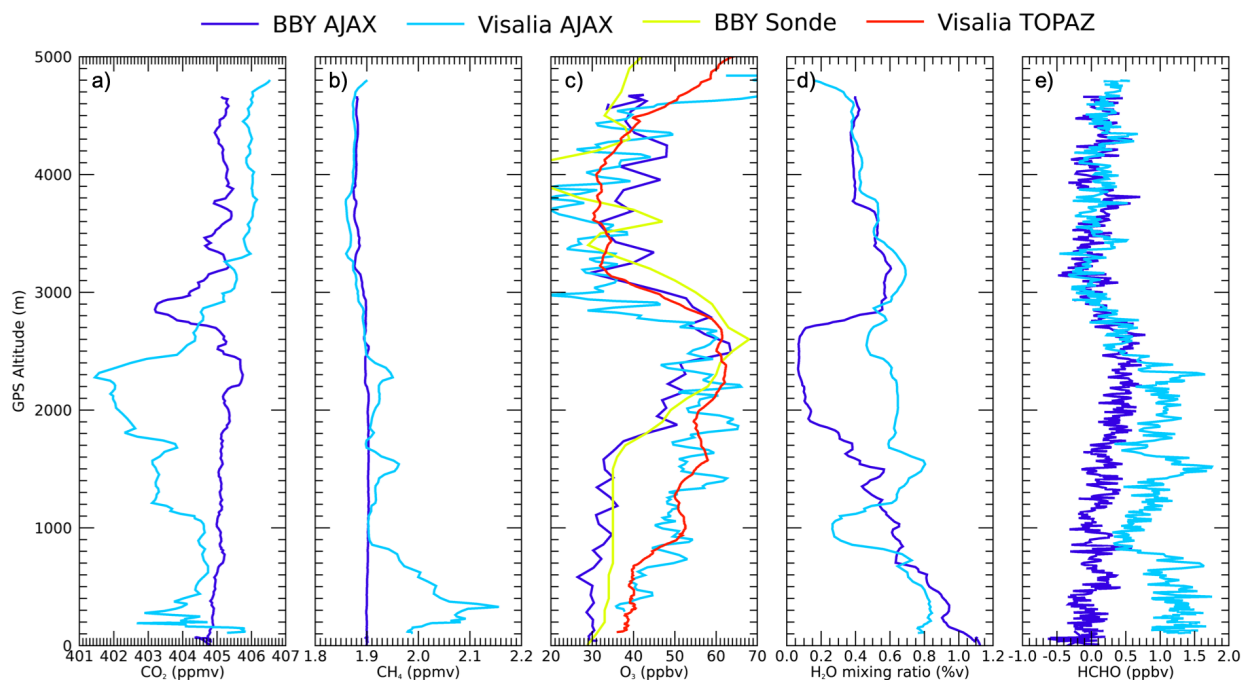

Fig. 10. The 15 June 2016 AJAX profiles taken at BBY and VMA (dark blue and light blue, respectively) of (a) CO_2, (b) methane, (c) ozone, (d) water vapor, and (e) formaldehyde. Aircraft profiles were measured at 1000 PDT at Bodega Bay and half an hour later at Visalia. The profiles of ozone measured by the ozonesondes at Bodega Bay (yellow) and from the TOPAZ lidar at Visalia (red) are superimposed in (c) for comparison.

slope sidewall venting is most active (Fast et al. 2012; Leukauf et al. 2016), injecting these two layers that wind up over Visalia on the morning of 15 June. These layers are more pronounced in CO_2 where they are characterized by drawdown from the agricultural photosynthesis of the valley environment, far more prevalent than where the particular CH_4 sources may have been. At the lowest levels, just above the Visalia airport and California Highway 99, the CO_2 signal exceeds the marine baseline due to fossil fuel combustion. HCHO also exhibits lofted plumes at 1,500 and 2,300 m over Visalia, similar to methane. Because the midday lifetime of HCHO due to photolysis and reaction with OH is only about 3 h (Choi et al. 2010), yet should be very long in the dark away from the surface, the presence of significant amounts of HCHO (up to 1.5 ppbv) shows that the lofting into the buffer layer is accomplished on the time scale of several hours over the course of any day.

The 15 June vertical profile measurements can be put into a larger perspective. Figure 11 superimposes the AJAX O_3 profile at Visalia from Fig. 10 on the TOPAZ time–height aerosol and ozone curtain plots. The curtain plots show relatively elevated O_3 extending above the ABL up to ~2,700 m, the top of the BuL. Different origins for these layers is consistent with the abrupt wind shift around 1.5 km. The buffer layer is capped by very clean air with less than 30 ppbv of O_3 and low aerosol backscatter. The absence of turbulence in this layer is reflected by the rapid loss in the wind profiler return signals, and veering of the winds to westerly flow, consistent with the climatological pressure field presented in Fig. 3, at the bottom of the clean layer (FT) can be seen. Above lies a 2-km-thick layer with >80 ppbv of O_3 (and low aerosol) consistent with transported Asian pollution. The superimposed AJAX profile in Fig. 11 shows that the aircraft sampled the very bottom of the transported pollution layer (not shown here, but exhibiting enhanced CO_2, HCHO, and CH_4) before descending into the clean layer.

Because CABOTS obtained many different vertical profiles of ozone across the state it is possible to look at how lower-tropospheric ozone layers correlate across large distances. As Parrish et al. (2010) point out, ozonesonde measurements aloft may correlate with various surface sites downwind in a wide lateral swath not due to direct parcel trajectories, but because ozone laminae that are commonly found in the lower troposphere often extend for hundreds of kilometers in the
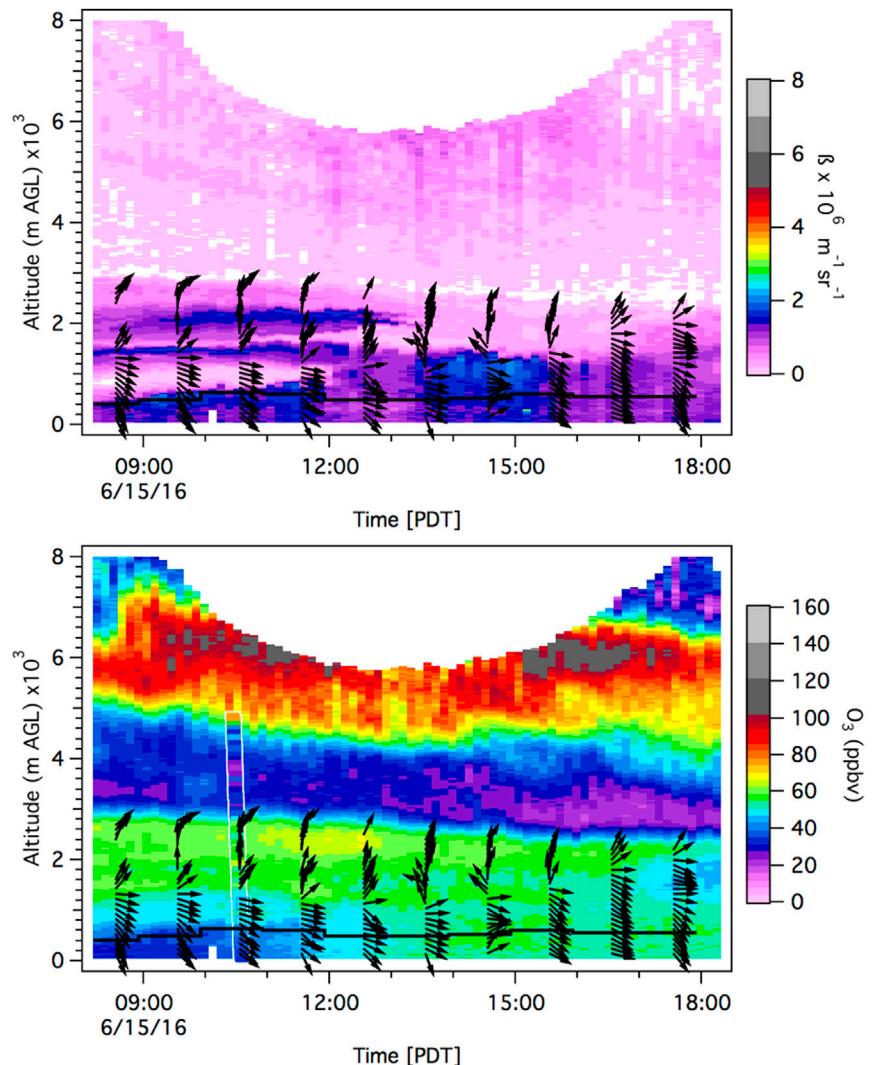
Fig. 11. Time–height curtain plots of the TOPAZ (top) aerosol backscatter and (bottom) ozone above the VMA with the collocated profiler winds and RASS boundary layer height. The AJAX ozone profile above the VMA is superimposed on the ozone plot (~1030–1040 PDT).

horizontal (Liu et al. 2009). Figure 12 shows the correlations between the two coastal ozonesonde sites 100 km apart for the 22 days with simultaneous launches. The layers seem to be spatially large enough to encompass both locations at altitudes between 1.5 and 2 km (near the altitude of the Chews Ridge observations), 4 km, and up near 6 km, with correlation coefficients of about 0.8. (the solid circles in Fig. 12 represent the correlations with P values less than 0.05.) The blue line of the left graph in Fig. 12 shows the correlations between the BBY ozonesondes and the fixed Chews Ridge measurements at the same hour 260 km south along the coast (the correlation coefficient is calculated between the surface measurement and each altitude bin of the ozonesonde and lidar). Here the observations at the mountain top site are influenced by dry deposition to the forests and experience some influences of the continental sources, but there is still a correlation of nearly 0.4 with air sampled between 0.8 and 1.2 km above Bodega Bay. The correlation between the mountain site at Chews Ridge and the Visalia lidar inland shows a pronounced peak just below 2.5 km (green dashed line; right axis) and supports the idea that the Chews Ridge observatory may serve as a decent monitor of the in-

flow air over the coast range that dilutes the ABL air that is lofted into the buffer layer over the SJV. And finally, the measurements that were taken the farthest apart, 400 km between BBY and Visalia, show some modest correlations at 4.5 and 1 km (red line; right panel.) The latter correlation near 0.5 corroborates the FLEXPART modeling results of Cooper et al. (2011) showing a strong influence of air parcels at 1 km above Point Reyes (~30 km south along the coast from BBY) and their receptor region covering the "south-central" SJV in dictating that flow above the marine ABL gets drawn into the sea/valley breeze circulation that affects the flow up to about 2 km in the valley.
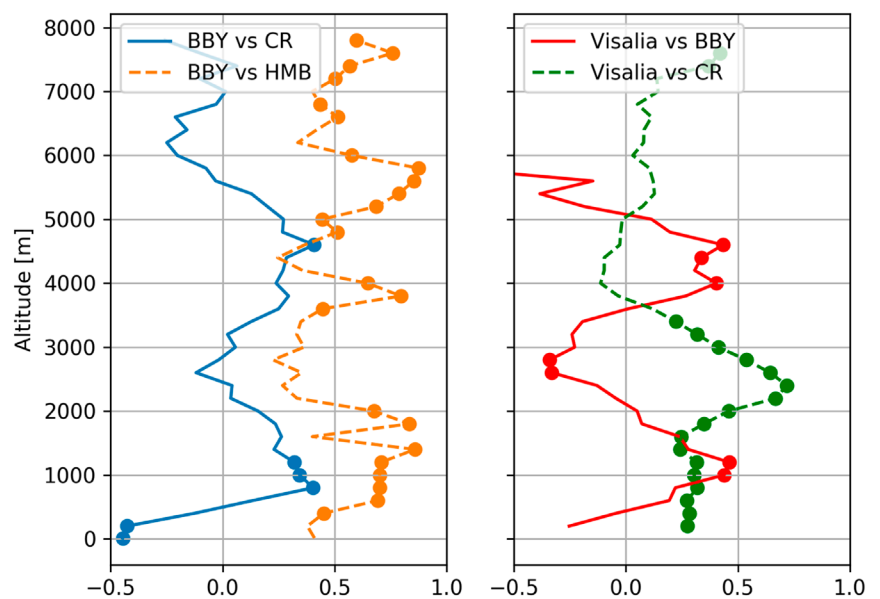
Fig. 12. (left) Correlation coefficients of Bodega Bay ozonesonde observations with coincident Chews Ridge surface ozone at 1.5 km (blue line) and Half Moon Bay ozonesonde measurements (orange dashed line). (right) Correlations of TOPAZ lidar data with Bodega Bay ozonesondes (red line) and Chews Ridge surface (green line). Circles represent correlations with p values < 0.05.

Summary

The collective observations of 440 h of O_3 lidar profiles over Visalia, over 100 coastal ozonesondes, and several targeted airborne surveys acquired during the 3-month CABOTS field experiment have the potential to greatly illuminate the meteorological mechanisms that determine the vertical distribution of O_3 above the central San Joaquin Valley. The high-temporal-resolution (daily for the coastal ozonesondes and daytime hourly for the lidar in the Central Valley) dataset should be able to provide novel constraints on modeling efforts, ultimately producing new insights into the transport and mixing processes contributing to the high surface O_3 levels found in this and other large valleys around the world. The lidar, RASS, and airborne measurements all confirmed the unusually shallow convective mixed layers of the SJV and the formation of a persistent buffer layer above the ABL between about 0.5 and 2.5 km. Because of the surrounding topography the buffer layer overlying the well-mixed boundary layer is made up of partially stagnating air polluted by regional surface sources

and a continuous dilution of incoming free-tropospheric air that contains a highly variable amount of exogenous ozone usually present in discrete layers.

The TOPAZ lidar also frequently detected elevated O_3 layers between 4 and 6 km above the valley floor consistent with biomass burning, transport from Asia, or descent from the lower stratosphere. Many of these layers most likely passed over the Sierra Nevada into the Intermountain West where they may have been entrained by the much deeper convective mixed layers that form in that hot, dry higher-elevation region (Langford et al. 2015, 2018).

The high-frequency daily ozonesondes showed a dramatic gradient in ozone reaching the coast from a median of 23 ppbv near the ocean surface and rising rapidly on average 17 ppb km^{-1} up to 2 km, consistent with rapid photochemical destruction in the summertime marine boundary layer. Above that strong gradient the average rise is an order of magnitude gentler (about 2 ppb km^{-1}), however the standard deviation increases aloft. The daily ozonesondes at Bodega Bay discovered the appearance of ozone concentrations below 3 km exceeding 70 ppbv, the 8-h ambient air quality standard, on average once every 5 days. Initial comparisons with a chemical transport model commonly used to provide the chemical boundary conditions at the North American coast indicate a low bias of about 10 ppbv in the lowest 3 km, below which the airflow dams up along the western edge of the southern Sierra Nevada mountains and potentially influences surface concentrations in California. The project dataset was fortunate to observe the coastal and valley air during several weeks of the Soberanes fire, a large wildfire that burned 130,000 acres (~526 km^2) in the coastal mountains over the course of nearly 3 months. The detailed observations of ozone in the complex terrain of the western United States is publicly available (at www.esrl.noaa.gov/csd/groups/csd3/measurements/cabots/) and may serve to challenge future modeling efforts that attempt to quantify the episodic trans-Pacific transport and impact of distant ozone sources on ongoing surface air quality violations in the mountainous west.

References

Alvarez, R. J., II, and Coauthors, 2011: Development and application of a compact, tunable, solid-state airborne ozone lidar system for boundary layer profiling. *J. Atmos. Oceanic Technol.*, **28**, 1258–1272, https://doi.org/10.1175/JTECH-D-10-05044.1.

Andreae, M. O., and P. Merlet, 2001: Emission of trace gases and aerosols from biomass burning. *Global Biogeochem. Cycles*, **15**, 955–966, https://doi.org/10.1029/2000GB001382.

Asher, E. C., and Coauthors, 2018: The transport of Asian dust and combustion aerosols and associated ozone to North America as observed from a mountaintop monitoring site in the California coast range. *J. Geophys. Res. Atmos.*, **123**, 5667–5680, https://doi.org/10.1029/2017JD028075.

Bao, J. W., S. A. Michelson, P. O. G. Persson, I. V. Djalalova, and J. M. Wilczak, 2008: Observed and WRF-simulated low-level winds in a high-ozone episode during the Central California Ozone Study. *J. Appl. Meteor. Climatol.*, **47**, 2372–2394, https://doi.org/10.1175/2008JAMC1822.1.

Beaver, S., and A. Palazoglu, 2009: Influence of synoptic and mesoscale meteorology on ozone pollution potential for San Joaquin Valley of California. *Atmos. Environ.*, **43**, 1779–1788, https://doi.org/10.1016/j.atmosenv.2008.12.034.

Bianco, L., I. V. Djalalova, C. W. King, and J. M. Wilczak, 2011: Diurnal evolution and annual variability of boundary-layer height and its correlation to other meteorological variables in California's Central Valley. *Bound.-Layer Meteor.*, **140**, 491–511, https://doi.org/10.1007/s10546-011-9622-4.

Brown-Steiner, B., and P. Hess, 2011: Asian influence on surface ozone in the United States: A comparison of chemistry, seasonality, and transport mechanisms. *J. Geophys. Res.*, **116**, D17309, https://doi.org/10.1029/2011JD015846.

Caiazzo, F., A. Ashok, I. A. Waitz, S. H. L. Yim, and S. R. H. Barrett, 2013: Air pollution and early deaths in the United States. Part I: Quantifying the impact of major sectors in 2005. *Atmos. Environ.*, **79**, 198–208, https://doi.org/10.1016/j.atmosenv.2013.05.081.

Caputi, D. J., I. Faloona, J. Trousdell, J. Smoot, N. Falk, and S. Conley, 2019: Residual layer ozone, mixing, and the nocturnal jet in California's San Joaquin Valley. *Atmos. Chem. Phys.*, **19**, 4721–4740, https://doi.org/10.5194/acp-19-4721-2019.

Choi, W., and Coauthors, 2010: Observations of elevated formaldehyde over a forest canopy suggest missing sources from rapid oxidation of arboreal hydrocarbons. *Atmos. Chem. Phys.*, **10**, 8761–8781, https://doi.org/10.5194/acp-10-8761-2010.

Conley, S. A., and Coauthors, 2011: A complete dynamical ozone budget measured in the tropical marine boundary layer during PASE. *J. Atmos. Chem.*, **68**, 55–70, https://doi.org/10.1007/s10874-011-9195-0.

——, I. C. Faloona, D. H. Lenschow, A. Karion, and C. Sweeney, 2014: A low-cost system for measuring horizontal winds from single-engine aircraft. *J. Atmos. Oceanic Technol.*, **31**, 1312–1320, https://doi.org/10.1175/JTECH-D-13-00143.1.

Cooper, O. R., and Coauthors, 2011: Measurement of western U.S. baseline ozone from the surface to the tropopause and assessment of downwind impact regions. *J. Geophys. Res.*, **116**, D00V03, https://doi.org/10.1029/2011JD016095.

Dorman, C. E., T. Holt, D. P. Rogers, and K. Edwards, 2000: Large-scale structure of the June–July 1996 marine boundary layer along California and Oregon. *Mon. Wea. Rev.*, **128**, 1632–1652, https://doi.org/10.1175/1520-0493(2000)128<1632:LSSOTJ>2.0.CO;2.

Emmons, L. K., and Coauthors, 2010: Description and evaluation of the Model for Ozone and Related chemical Tracers, version 4 (MOZART-4). *Geosci. Model Dev.*, **3**, 43–67, https://doi.org/10.5194/gmd-3-43-2010.

EPA, 1970: Summary of the Clean Air Act 42 U.S.C. §7401 et seq. (1970), www.epa.gov/laws-regulations/summary-clean-air-act.

——, 2013: Integrated Science Assessment (ISA) of Ozone (O3) and related photochemical oxidants. Tech. Rep. EPA/600/R-10/076F, 1251 pp.

Faloona, I., 2018: Ozone in the lower atmosphere and its contribution to high ozone concentrations at ground-level in the Southern San Joaquin Valley. ARB Tech. Rep. 14-308, 71 pp.

Fast, J. D., and Coauthors, 2012: Transport and mixing patterns over Central California during the Carbonaceous Aerosol and Radiative Effects Study (CARES). *Atmos. Chem. Phys.*, **12**, 1759–1783, https://doi.org/10.5194/acp-12-1759-2012.

Hamill, P., L. T. Iraci, E. L. Yates, W. Gore, T. P. Bui, T. Tanaka, and M. Loewenstein, 2016: A new instrumented airborne platform for atmospheric research. *Bull. Amer. Meteor. Soc.*, **97**, 397–404, https://doi.org/10.1175/BAMS-D-14-00241.1.

HTAP, 2010: Hemispheric transport of air pollution 2010. Part A: Ozone and particulate matter. Air Pollution Studies 17, United Nations, 278 pp.

Hudman, R. C., and Coauthors, 2004: Ozone production in transpacific Asian pollution plumes and implications for ozone air quality in California. *J. Geophys. Res.*, **109**, D23S10, https://doi.org/10.1029/2004JD004974.

Jacob, D. J., J. A. Logan, and P. P. Murti, 1999: Effect of rising Asian emissions on surface ozone in the United States. *Geophys. Res. Lett.*, **26**, 2175–2178, https://doi.org/10.1029/1999GL900450.

Jaffe, D. A., and N. L. Wigder, 2012: Ozone production from wildfires: A critical review. *Atmos. Environ.*, **51**, 1–10, https://doi.org/10.1016/j.atmosenv.2011.11.063.

——, and Coauthors, 1999: Transport of Asian air pollution to North America. *Geophys. Res. Lett.*, **26**, 711–714, https://doi.org/10.1029/1999GL900100.

——, and Coauthors, 2018: Scientific assessment of background ozone over the U.S.: Implications for air quality management. *Elem. Sci. Anth.*, **6**, 56, https://doi.org/10.1525/ELEMENTA.309.

Kley, D., P. Crutzen, H. Smit, H. Vömel, S. Oltmans, H. Grassl, and V. Ramanathan, 1996: Observations of near-zero ozone concentrations over the convective Pacific: Effects on air chemistry. *Science*, **274**, 230–233, https://doi.org/10.1126/science.274.5285.230.

Landrigan, P. J., and Coauthors, 2018: The Lancet Commission on pollution and health. *Lancet*, **391**, 462–512, https://doi.org/10.1016/S0140-6736(17)32345-0.

Langford, A. O., and Coauthors, 2015: An overview of the 2013 Las Vegas Ozone Study (LVOS): Impact of stratospheric intrusions and long-range transport on surface air quality. *Atmos. Environ.*, **109**, 305–322, https://doi.org/10.1016/j.atmosenv.2014.08.040.

——, and Coauthors, 2017: Entrainment of stratospheric air and Asian pollution by the convective boundary layer in the southwestern U.S. *J. Geophys. Res. Atmos.*, **122**, 1312–1337, https://doi.org/10.1002/2016JD025987.

——, and Coauthors, 2018: Coordinated profiling of stratospheric intrusions and transported pollution by the Tropospheric Ozone Lidar Network (TOLNet) and NASA Alpha Jet experiment (AJAX): Observations and comparison to HYSPLIT, RAQMS, and FLEXPART. *Atmos. Environ.*, **174**, 1–14, https://doi.org/10.1016/j.atmosenv.2017.11.031.

——, and Coauthors, 2019: Intercomparison of lidar, aircraft, and surface ozone measurements in the San Joaquin Valley during the California Baseline Ozone Transport Study (CABOTS). *Atmos. Meas. Tech.*, **12**, 1889–1904, https://doi.org/10.5194/amt-12-1889-2019.

Lapina, K., D. K. Henze, J. B. Milford, and K. Travis, 2016: Impacts of foreign, domestic, and state-level emissions on ozone-induced vegetation loss in the United States. *Environ. Sci. Technol.*, **50**, 806–813, https://doi.org/10.1021/acs.est.5b04887.

Leukauf, D., A. Gohm, and M. W. Rotach, 2016: Quantifying horizontal and vertical tracer mass fluxes in an idealized valley during daytime. *Atmos. Chem. Phys.*, **16**, 13049–13066, https://doi.org/10.5194/acp-16-13049-2016.

Li, J., A. Mahalov, and P. Hyde, 2016: Impacts of agricultural irrigation on ozone concentrations in the Central Valley of California and in the contiguous United States based on WRF-Chem simulations. *Agric. For. Meteor.*, **221**, 34–49, https://doi.org/10.1016/j.agrformet.2016.02.004.

Liang, Q., L. Jaeglé, D. A. Jaffe, P. Weiss-Penzias, A. Heckman, and J. A. Snow, 2004: Long-range transport of Asian pollution to the northeast Pacific: Seasonal variations and transport pathways of carbon monoxide. *J. Geophys. Res.*, **109**, D23S07, https://doi.org/10.1029/2003JD004402.

Lin, M. Y., and Coauthors, 2012a: Springtime high surface ozone events over the western United States: Quantifying the role of stratospheric intrusions. *J. Geophys. Res.*, **117**, D00V22, https://doi.org/10.1029/2012JD018151.

——, and Coauthors, 2012b: Transport of Asian ozone pollution into surface air over the western United States in spring. *J. Geophys. Res.*, **117**, D00V07, https://doi.org/10.1029/2011JD016961.

——, L. W. Horowitz, S. J. Oltmans, A. M. Fiore, and S. M. Fan, 2014: Tropospheric ozone trends at Mauna Loa Observatory tied to decadal climate variability. *Nat. Geosci.*, **7**, 136–143, https://doi.org/10.1038/ngeo2066.

Lin, Y. L., and I. C. Jao, 1995: A numerical study of flow circulations in the Central Valley of California and formation mechanisms of the Fresno eddy. *Mon. Wea. Rev.*, **123**, 3227–3239, https://doi.org/10.1175/1520-0493(1995)123<3227:ANSOFC>2.0.CO;2.

Liu, G. P., D. W. Tarasick, V. E. Fioletov, C. E. Sioris, and Y. J. Rochon, 2009: Ozone correlation lengths and measurement uncertainties from analysis of historical ozonesonde data in North America and Europe. *J. Geophys. Res.*, **114**, D04112, https://doi.org/10.1029/2008JD010576.

McConnell, R., and Coauthors, 2002: Asthma in exercising children exposed to ozone: A cohort study. *Lancet*, **359**, 386–391, https://doi.org/10.1016/S0140-6736(02)07597-9.

Myhre, G., and Coauthors, 2013: Anthropogenic and natural radiative forcing. *Climate Change 2013: The Physical Science Basis,* T. F. Stocker et al., Eds., Cambridge University Press, 659–740.

Oltmans, S. J., A. S. Lefohn, J. M. Harris, and D. S. Shadwick, 2008: Background ozone levels of air entering the west coast of the US and assessment of longer-term changes. *Atmos. Environ.*, **42**, 6020–6038, https://doi.org/10.1016/j.atmosenv.2008.03.034.

Panek, J., D. Saah, A. Esperanza, A. Bytnerowicz, W. Fraczek, and R. Cisneros, 2013: Ozone distribution in remote ecologically vulnerable terrain of the southern Sierra Nevada, CA. *Environ. Pollut.*, **182**, 343–356, https://doi.org/10.1016/j.envpol.2013.07.028.

Parrish, D. D., K. C. Aikin, S. J. Oltmans, B. J. Johnson, M. Ives, and C. Sweeny, 2010: Impact of transported background ozone inflow on summertime air quality in a California ozone exceedance area. *Atmos. Chem. Phys.*, **10**, 10093–10109, https://doi.org/10.5194/acp-10-10093-2010.

——, and Coauthors, 2014: Long-term changes in lower tropospheric baseline ozone concentrations: Comparing chemistry-climate models and observations at northern midlatitudes. *J. Geophys. Res. Atmos.*, **119**, 5719–5736, https://doi.org/10.1002/2013JD021435.

——, L. M. Young, M. H. Newman, K. C. Aikin, and T. B. Ryerson, 2017: Ozone design values in Southern California's air basins: Temporal evolution and US background contribution. *J. Geophys. Res. Atmos.*, **122**, 11166–11182, https://doi.org/10.1002/2016JD026329.

Pfister, G. G., and Coauthors, 2011: Characterizing summertime chemical boundary conditions for airmasses entering the US West Coast. *Atmos. Chem. Phys.*, **11**, 1769–1790, https://doi.org/10.5194/acp-11-1769-2011.

Pusede, S. E., and Coauthors, 2014: On the temperature dependence of organic reactivity, nitrogen oxides, ozone production, and the impact of emission controls in San Joaquin Valley, California. *Atmos. Chem. Phys.*, **14**, 3373–3395, https://doi.org/10.5194/acp-14-3373-2014.

Russell, L. M., and Coauthors, 1998: Bidirectional mixing in an ACE 1 marine boundary layer overlain by a second turbulent layer. *J. Geophys. Res.*, **103**, 16411–16432, https://doi.org/10.1029/97JD03437.

Ryerson, T. B., and Coauthors, 2013: The 2010 California Research at the Nexus of Air Quality and Climate Change (CalNex) field study. *J. Geophys. Res. Atmos.*, **118**, 5830–5866, https://doi.org/10.1002/JGRD.50331.

Sindelarova, K., and Coauthors, 2014: Global data set of biogenic VOC emissions calculated by the MEGAN model over the last 30 years. *Atmos. Chem. Phys.*, **14**, 9317–9341, https://doi.org/10.5194/acp-14-9317-2014.

Škerlak, B., M. Sprenger, and H. Wernli, 2014: A global climatology of stratosphere–troposphere exchange using the ERA-Interim data set from 1979 to 2011. *Atmos. Chem. Phys.*, **14**, 913–937, https://doi.org/10.5194/acp-14-913-2014.

Sprenger, M., and H. Wernli, 2003: A northern hemisphere climatology of cross-tropopause exchange for the ERA15 time period (1979-1993). *J. Geophys. Res.*, **108**, 8521, https://doi.org/10.1029/2002JD002636.

St. Clair, J. M., A. K. Swanson, S. A. Bailey, G. M. Wolfe, J. E. Marrero, L. T. Iraci, J. G. Hagopian, and T. F. Hanisco, 2017: A new non-resonant laser-induced fluorescence instrument for the airborne in situ measurement of formaldehyde. *Atmos. Meas. Tech.*, **10**, 4833–4844, https://doi.org/10.5194/amt-10-4833-2017.

Stevenson, D. S., and Coauthors, 2006: Multimodel ensemble simulations of present-day and near-future tropospheric ozone. *J. Geophys. Res.*, **111**, D08301, https://doi.org/10.1029/2005JD006338.

Sun, W., M. Shao, C. Granier, Y. Liu, C. S. Ye, and J. Y. Zheng, 2018: Long-term trends of anthropogenic SO_2, NO_x, CO, and NMVOCs emissions in China. *Earth's Future*, **6**, 1112–1133, https://doi.org/10.1029/2018EF000822.

Trousdell, J. F., S. A. Conley, A. Post, and I. C. Faloona, 2016: Observing entrainment mixing, photochemical ozone production, and regional methane emissions by aircraft using a simple mixed-layer framework. *Atmos. Chem. Phys.*, **16**, 15433–15450, https://doi.org/10.5194/acp-16-15433-2016.

——, D. Caputi, J. Smoot, S. A. Conley, and I. C. Faloona, 2019: Photochemical production of ozone and emissions of NOx and CH4 in the San Joaquin Valley. *Atmos. Chem. Phys.*, **19**, 10697–10716, https://doi.org/10.5194/acp-19-10697-2019.

Verstraeten, W. W., J. L. Neu, J. E. Williams, K. W. Bowman, J. R. Worden, and K. F. Boersma, 2015: Rapid increases in tropospheric ozone production and export from China. *Nat. Geosci.*, **8**, 690–695, https://doi.org/10.1038/ngeo2493.

Vinken, G. C. M., K. F. Boersma, J. D. Maasakkers, M. Adon, and R. V. Martin, 2014: Worldwide biogenic soil NO_x emissions inferred from OMI NO_2 observations. *Atmos. Chem. Phys.*, **14**, 10363–10381, https://doi.org/10.5194/acp-14-10363-2014.

Westerling, A. L., H. G. Hidalgo, D. R. Cayan, and T. W. Swetnam, 2006: Warming and earlier spring increase western US forest wildfire activity. *Science*, **313**, 940–943, https://doi.org/10.1126/SCIENCE.1128834.

Yates, E. L., and Coauthors, 2017: An assessment of ground level and free tropospheric ozone over California and Nevada. *J. Geophys. Res. Atmos.*, **122**, 10089–10102, https://doi.org/10.1002/2016JD026266.

Young, P. J., and Coauthors, 2013: Pre-industrial to end 21st century projections of tropospheric ozone from the Atmospheric Chemistry and Climate Model Intercomparison Project (ACCMIP). *Atmos. Chem. Phys.*, **13**, 2063–2090, https://doi.org/10.5194/acp-13-2063-2013.

Zardi, D., and C. D. Whiteman, 2013: Diurnal mountain wind systems. *Mountain Weather Research and Forecasting: Recent Progress and Current Challenges*, F. K. Chow, S. F. J. De Wekker, and B. J. Snyder, Eds., Springer, 35–119.

Zhang, X., X. Chen, and X. Zhang, 2018: The impact of exposure to air pollution on cognitive performance. *Proc. Natl. Acad. Sci. USA*, **115**, 9193–9197, https://doi.org/10.1073/pnas.1809474115.

Zhang, X.-J., J. H. Helsdon, and R. D. Farley, 2003: Numerical modeling of lightning-produced NO_x using an explicit lightning scheme: 1. Two-dimensional simulation as a "proof of concept." *J. Geophys. Res.*, **108**, 4579, https://doi.org/10.1029/2002JD003224.

Zhong, S. Y., C. D. Whiteman, and X. D. Bian, 2004: Diurnal evolution of three-dimensional wind and temperature structure in California's Central Valley. *J. Appl. Meteor.*, **43**, 1679–1699, https://doi.org/10.1175/JAM2154.1.

Ziemke, J. R., B. N. Chandra, L. Duncan, P. K. Froidevaux, P. K. Bhartia, P. F. Levelt, and J. W. Waters, 2006: Tropospheric ozone determined from Aura OMI and MLS: Evaluation of measurements and comparison with the global modeling initiative's chemical transport model. *J. Geophys. Res.*, **111**, D19303, https://doi.org/10.1029/2006JD007089.